Characteristics of micro hot-film probes for aeronautical purposes

Tobias Beutel#, Christoph Boese, Christoph Luzemann, Ansgar Holle, Monika Leester-Schädel and Stephanus Büttgenbach

Institute for Microtechnology (IMT), Technische Universität Braunschweig, Alte Salzdahlumer Straße 203, 38124 Braunschweig, Germany
E-mail: T.Beutel@TU-Braunschweig.de, TEL: +49-(0)531-391-9748, FAX: +49-(0)531-391-9751

KEYWORDS: flow measurement, hot-film, AeroMEMS, micro system technology, wall-shear stress.

In this work we present the design, fabrication and characterization of AeroMEMS hot-film probes. The hot-films are structured on glass or silicon substrates using silicon bulk-micromachining processes. For the initial tests, different metal layers e.g. gold, aluminum, titanium and nickel are magnetron sputtered onto wafer substrates. These hot-films have a variety of geometries and are developed for special measurements of wall-shear stress in fluid mechanics. This study discusses the failures introduced by geometry effects which occur due to isotropic wet etching of the metal layers. Also presented are the non-dynamic and dynamic test procedures used to characterize the hot-film probes. It was discovered that by varying the length and the material, varying electrical properties can be obtained. The determined material constants vary from those known from the bulk material. Dynamic tests in the desktop wind tunnel are also described and the measurement of the heat conduction from the hot-film through the substrate and its influence on the maximum operating frequency is discussed. In the long-term view, hot-films in combination with a pressure sensor on the same chip should be able to detect the state of the flow (laminar or turbulent).

Manuscript received: March XX, 2011 / Accepted: January XX, 2011

NOMENCLATURE

α	= temperature coefficient	$[1/K]$
b	= width of the hot-film	$[m]$
l	= length of the hot-film	$[m]$
h	= height of the hot-film	$[m]$
A	= area of the hot-film	$[m^2]$
P	= electrical power	$[W]$
$\dot{Q}$	= heat transfer	$[W]$
v	= velocity	$[m/s]$
ρ	= elec. Resistivity or density	$[\Omega m]$ or $[kg/m^3]$
θ	= temperature difference	$[K]$

Indices:

0 for ambient; *S* for operating temperature; *H* for hot-film; *corr* for corrected; *F* for fluid; *I* for Input; *O* for Output

1. Introduction

Due to the ever increasing costs of energy, as well as aspects of environmental protection, ever more efficient products must be developed. Therefore, in the aeronautical industry, it is necessary to continually investigate new concepts to reduce the fuel consumption and noise emission of civil aircraft.

In a new approach to active high lift, the use of controlled suction and blow out of compressed air at defined locations along the wing, including a coanda flap, is expected to significantly reduce pressure drag. This concept is based on the ability to measure the state of the flow and to be able to control it in real time. With new piezoceramic actuators, which make small changes to their length under high voltage excitation, it is possible to change the contour of wing sections. Specifically, the height of the blow-out slot is expected to be actuated at the needed frequency. In this way, the near wall flow velocity on the coanda flap is accelerated in order to maintain laminar flow along as much of the wing chord as possible and thereby produce a high lift coefficient (C_A). The required mass flow of pressurized air for the controlled system is expected to be low. This concept is expected to be comparable or more effective than common high lift systems. To enable effective high-lift, the control frequency of the complete closed-loop sensing and actuating system is expected to be higher than 100 *Hz*.

These requirements lead to new sensors which are capable of determining the state of the flow, without influencing it. Due to economic and technological constraints it is advisable to use carbon fiber laminate for the wings skin. Micro-fabricated sensors (AeroMEMS) can be implemented into the wing skin enabling space resolved measurements [BEU10].

An integral part of the presented sensing element is the hot-film sensor. This sensor was designed and tested for the application described above. In this article the sensor development will be described with consideration to the sensor design and the initial tests.

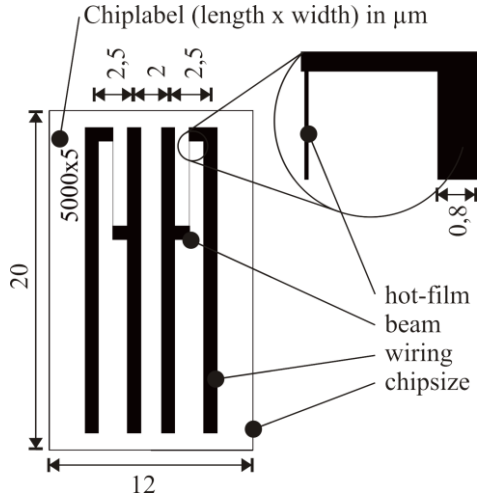

Fig. 1: Drawing of the test structures with dimensions
(all dimensions in *mm*, except of the chip label, which is in μm)

Several layouts based on various materials will be introduced. The influence of these parameters on the static and dynamic behavior will be compared. In particular, the effect of various materials used for the hot-film and the substrate will be discussed.

At the end of the manuscript a brief outlook is provided to give an impression of future activities in this field.

2. Sensor Design and Fabrication

As these sensors are the very first hot-films fabricated at the Institute for Microtechnology (IMT), it was decided to use a universal form. As shown in Figure 1, a wire pitch similar to USB A norm was chosen. This enables the sensors to be plugged into USB female connectors, making changes simple.

The length l of the hot-film depends on the distance between the two beams leading from the wiring to the hot-film. The wiring is designed symmetrically in order to be more flexible. The length has been varied from 1000 to 8000 μm. The width of the wiring was set to 800 μm, while the width b of the hot-film was varied in steps of 1 μm between 5 and 10 μm. These values are valid for the lithographic mask, which will be shown later.

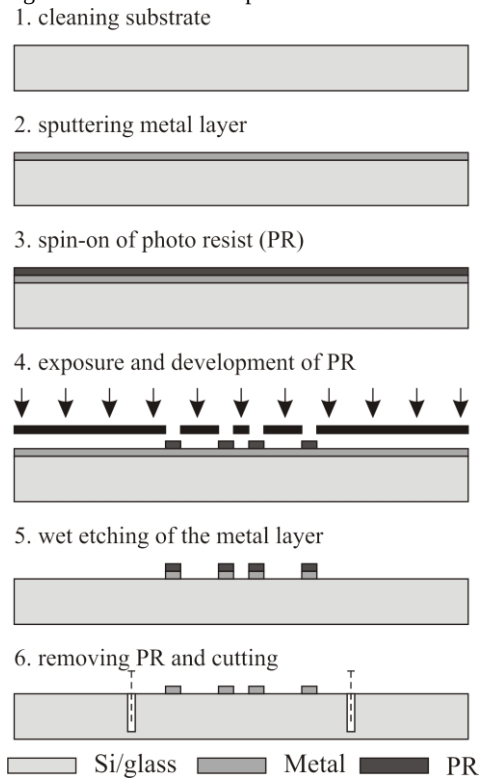

Fig. 2: Scheme of process steps during micro fabrication

20 of these test structures were distributed on a 4" wafer made of glass or (100)-silicon. Due to fabrication issues, the narrower films are placed near the center.

The fabrication process has been developed specifically for this design. The sensor has been fabricated in a batch process using state-of-the-art microsystem technologies. The figure mentioned above shows a simplified scheme of the most significant steps during the process.

After cleaning the substrate (1), the glass wafers are dehydrated. The metal layer is then magnetron sputtered (2) directly onto the substrate. No reverse sputtering (etching) was carried out, which is normally is used to obtain improved ohmic contact to underlying layers, but for this case is not necessary.

The thickness of the sputtered metal layer determines the resulting height of the film h . This thickness depends on the duration of magnetron sputtering and on the power applied. Furthermore, the sputtering rates strongly depend on the target material. The thickness has to be evaluated for each material. Optimization processes can be carried out in order to achieve a homogeneous thickness over the entire wafer. For these tests we used the programs listed in Table 1, which lead to the given nominal metal layer thicknesses.

material	nom. thickness
Gold (Au)	275 *nm*
Aluminum (Al)	600 *nm*
Titanium (Ti)	154 *nm*
Nickel (Ni)	194 *nm*

Table 1: Material and nominal thickness of the metal layers depending on the program for magnetron sputtering machine

The given thicknesses in the second column are some of the most important values for these sensors, as they directly influence the electrical behavior.

After sputtering, a photolithographic process (3 & 4) has to be carried out in order to cover the desired metal layer positions with positive photo resist (PR). A metal specific wet etching process (5) is then used to structure the hot-films. Finally, the PR is removed and the wafers are diced in order to obtain the individual chips.

Wet-etching of metal layers is an isotropic process. This means that the etching rates in all spatial directions are equal. Due to the small dimensions of the design the effective conducting cross-section of the metal is significantly reduced. Figure 3 shows the geometry parameters.

The corrected conducting area A_{corr} can be calculated as follows:

$$A_{corr} = bh - \frac{1}{2}\pi h^2$$

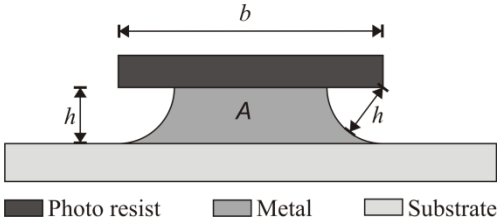

Fig. 3: Cross-section of a wet-etched hot-wire

This underetching can reduce up to 20 % of the conducting area, which impacts the sensor´s behavior. In practice this deviation is further amplified, due to the fact that the etching process is conducted over the entire wafer. The etching process typically starts from the wafer border moving to the center. This leads to a radius higher than h when the etching time is exceeded, especially in the outer regions.

Deviation in the length is not as significant, because l is much larger than h. The corrected length l_{corr} can be calculated by $l_{corr} = l + 2h$ in the first approximation. Fig. 4 shows the profile of a cut hot-film. The rounded etch edge expected from the theory is not clearly identifiable. This leads to uncertainty in the calculation of the conducting area A_{corr}.

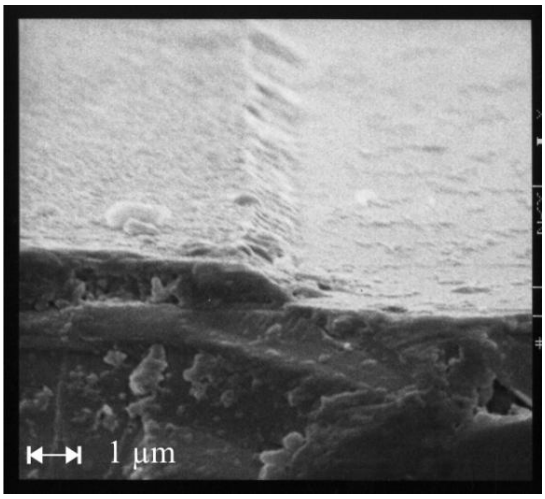

Fig. 4: REM picture of an hot-film (aluminum on silicon)

3. Sensor Characterization

The following formula is a fundamental equation for hot-film anemometers describing the relationship between the temperature and the resistance of the film:

$$R_s = R_0[1 + \alpha(T_S - T_0)] = R_0[1 + \alpha\theta]$$

where R is the electrical resistance and T is the temperature at ambient (index *0*) or at operating condition (index *S*). α represents the temperature coefficient while θ is the temperature difference between T_S and T_0. This is needed to obtain a heat transfer $\dot{Q}$ via forced convection from the metal film into the fluid having the velocity v. The electrical power P applied to the hot-film must be equal to the heat transfer $\dot{Q}$. This relationship was first described by King [KIN14] and does not include any losses.

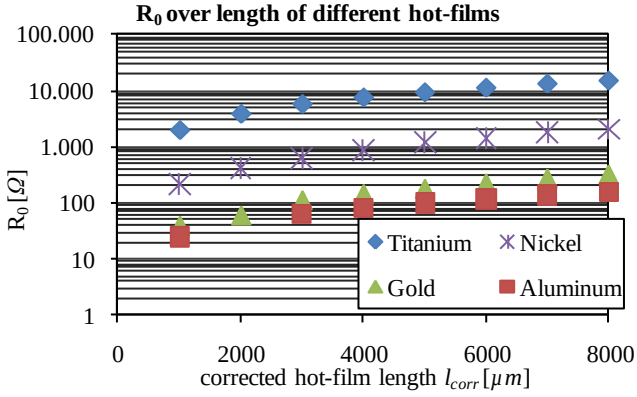

Fig. 5: Resistance at ambient temperature R_0 over hot-film length of different materials ($b = 7\ \mu m$, h according to Table 1)

$$P(I, R_H) = \dot{Q}(\rho_F, v, \theta)$$

In the application described here, the density of the fluid ρ_F and its temperature T_F are constant. Depending on the measuring methods used, either R_H, θ or I are kept constant. The most frequently used measuring concepts are described in section 3.2.

Several tests have been carried out to measure the characteristics of the hot-film sensors and its components. The first tests were non-dynamic, where no fluids or fast changing conditions were used. Subsequent dynamic tests were performed, using various electrical circuits for anemometry.

3.1 Static Characteristics of the prototypes

The resistance of the hot-film at ambient temperature R_0 is simple to measure. In order to make sure that θ can be calculated correctly, the ambient temperature must be measured simultaneously. Figure 5 shows the resistance R_0 depending on the material, its thickness and its length. The linear relationship between the length l and the resistance R_0 can be expressed by $y = mx + c$, where the offset c represents the zero sequence resistance between two measurement points at a theoretical hot-film length of zero.

The following equation shows the relationship between the geometric parameters and the electrical resistivity ρ, which is a material constant normally defined at 20 °C.

$$R_0 = \rho \frac{l}{A}$$

From this equation it is possible to calculate ρ from the conducting area A_{corr} and the length of the hot-film l_{corr}. The results of these measurements are shown in Table 2. Although the corrected values are used for calculation, some deviation may occur due to practical etching procedures. For this reason A_{corr} can not be precisely calculated in practice.

Material	Resistivity ρ_{20} [Ωm] from experiments	Resistivity ρ_{20} [Ωm] from literature	
Gold Au	$6{,}46 \cdot 10^{-8}$	$2{,}20 \cdot 10^{-8}$ $2{,}44 \cdot 10^{-8}$	[HER08] [ASM90]
Aluminum Al	$7{,}45 \cdot 10^{-8}$	$2{,}70 \cdot 10^{-8}$ $2{,}82 \cdot 10^{-8}$	[HER08] [ASM90]
Titanium Ti	$1{,}97 \cdot 10^{-6}$	$4{,}20 \cdot 10^{-7}$ $5{,}20 \cdot 10^{-7}$	[ASM90]
Nickel Ni	$2{,}97 \cdot 10^{-7}$	$9{,}50 \cdot 10^{-7}$	[FAR68]

Table 2: Determination of the electrical resistivity ρ_{20} in comparison with values from literature

Table 2 shows a large discrepancy between the values given in literature and the obtained results. Because these values were measured accurately and repeatedly, this disparity cannot be explained completely. In our calculations of the gold hot-films, the underlying 10 *nm* chrome layers which were used to increase adhesion to the glass substrate, were not taken into consideration.

To measure the resistance at operating temperature R_S, another set-up was used. The goal was to identify the temperature coefficient α, therefore an infrared camera was installed in front of the hot-film probes. A constant voltage supply module was used to feasibly regulate the hot-film`s temperature. The hot-film had to be sealed so that no air movement was able to disturb the measurement. For every applied voltage U_I the temperature T_S and the current I_O was measured. Because of the limitation of the camera, no temperature above 240 °C could be measured. The resistance R_S at

operating temperature can be calculated by $R_s = U/I$.

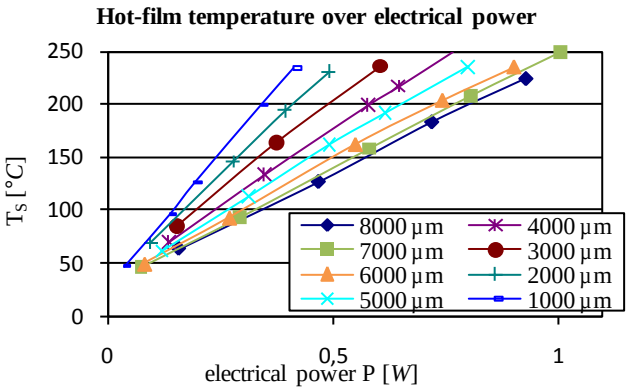

Fig. 6: Temperature over electrical power at different lengths ($b = 10\ \mu m$; Au)

Figure 6 shows the resulting temperatures for the hot-films ($b = 10\ \mu m$; Gold) depending on their length. One can see that the difference between the resistance R_0 and the resistance R_S at higher temperatures increases for longer hot-films. The slope of these results is important because it describe how the output signal depends on the change of resistance. The influence of R_0 on the measurement accuracy of increasing lengths with constant cross-sections can be determined from the following equation:

$$R_s = R_0[1 + \alpha\theta] = \rho\frac{l}{A}[1 + \alpha\theta]$$

From this equation we are able to determine that increased length as well as even thinner hot-films lead to improved sensor sensitivity.

3.2 Test system set-up for dynamic tests

This section describes the preliminary dynamic tests of the hot-films. These tests were the first to be conducted, and the set-up was improved frequently to obtain even more precise and reliable test results.

The test set-up consists of a fan which can be regulated by increasing the supply voltage from 0 to 220 V AC. The voltage can be seen as an index for the air speed. Within the tunnel a flow straightener was used to refine the flow profile. The entire set-up is roughly 1 m long, so that it may easily fit on a desktop, which should be located in an air-conditioned laboratory to avoid temperature drift.

As known from literature, three sorts of electrical circuits are common to operate hot-films:

- Constant Temperature Anemometry (CTA), where the temperature of the hot-film is kept constant [TRO07].
- Constant Current Anemometry (CCA), where the current through the hot-film is kept constant while the resistance of the film is measured [TRO07].
- Constant Voltage Anemometry (CVA) where the voltage drop along the hot-film is kept constant.

In this work CTA and CVA methods were used. For these tests, separate printed circuit boards (PCB) were designed.

In both circuits R_H was used to represent the hot-film resistance. The resistors R_A and R_B were applied to construct a quarter-bridge including the hot-film and a potentiometer R_{var}.

In the CTA method (Fig. 7) the potentiometer is used to adjust the hot-film's operation temperature before measurement. An infrared camera (IR sensitive) was used to measure the hot-film`s temperature. After a very short stabilization process the output current I_O becomes constant and measurements can be performed. If the hot-film is cooled due to a flow, the amplifier increases the current, leading to a constant hot-film temperature The circuit is driven by the voltage applied from the operational amplifier.

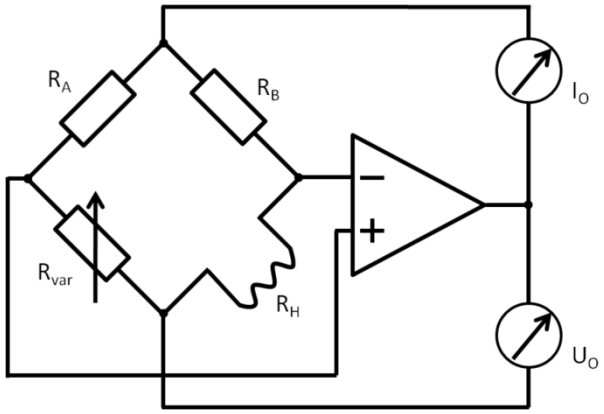

Fig. 7: Circuit used for CTA.

In the CCA method (Fig. 8) a constant voltage U_{Source} is applied to produce a constant current to heat the hot-film. By changing the resistance R_{var} the operation temperature can be set. After adjusting R_{var}, the trimmer R_m has to be tuned until a constant current is applied and U_O is stable.

Because of the relatively high sensitivity of this set-up, all resistors should be suitable for high loads in order to reduce the disturbing effects of temperature drift. The hot-film is cooled due to the flow over the hot-film, leading to a resistivity decrease. Hence the

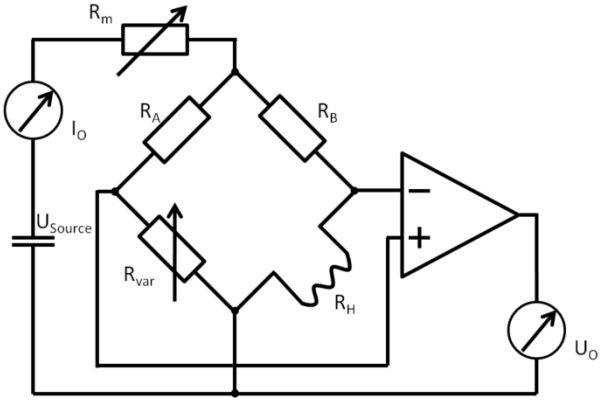

Fig. 8: Circuit used for CCA

output voltage U_O increases, producing the signal to be measured.

In the CVA circuit the core components are nearly the same, except that the voltage drop along the hot-film is held constant instead of the current. This makes the circuit more robust to electromagnetic influences. The circuit is connected to a constant voltage supply and the amplifier is used as an inverting amplifier. When a flow cools the hot-film, the operational amplifier increases its output voltage. Thereby the output current must also increase. Both values are used to calculate the electrical power $P = U_O I_O$.

In literature several discussions for and against a particular circuit can be found, and therefore all versions were investigated. In CTA mode the sensor cannot be overheated unintentionally making the CTA preferable. Unfortunately, this method provides relatively small changes in the output at high flow rates [ECK 97].

According to literature, CCA provides good results at low fluid velocities. On the other hand, fluctuations can lead to sensor inaccuracies. Hence, the minimum velocity and maximum power, are limited, leading to a narrow band of velocities where CCA is optimal.

3.3 Determination of the static heat allocation in the substrate

In this section different issues affecting the range of the heat allocation are discussed. The heat generated by the hot-film, spreads into both the fluid and the substrate. It is important to consider this effect in the designing process of a hot-film sensor, especially if the sensor is integrated in a module of several sensing elements where it could interact with the other sensing modules. The dynamic properties of the hot-film are also influenced by heat allocation. These effects have lead to an extensive thermal investigation to develop a sensor with a well known and highly dynamic behavior.

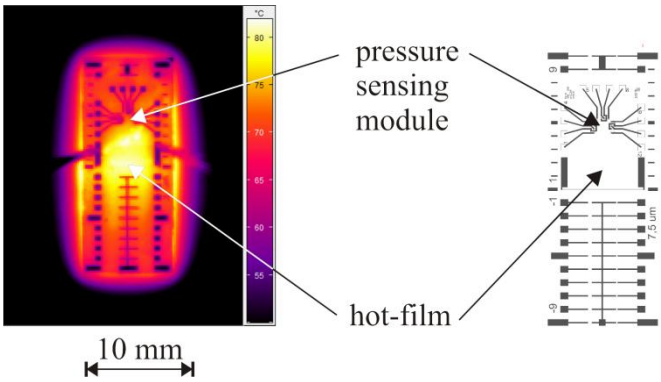

Fig. 9: Picture taken by infrared sensitive camera (left) and sketch of the chip (right)

Keeping in mind that the manufactured hot-films mentioned above are deposited and structured directly onto substrate, effective heat conduction is present. Consequently, the heat transfer from the hot-film can not only be solved for the convective heat transfer. The convective heat transfer can be indirectly used to determine the flow velocity. If the conductive heat transfer exceeds the convective heat transfer, the ratio of desired signal to the real output signal will be reduced [NIT06]. Therefore, either the conductive heat transfer has to be reduced or the measurement frequency of the hot-film has to be high enough to filter out the slow reacting substrate influences.

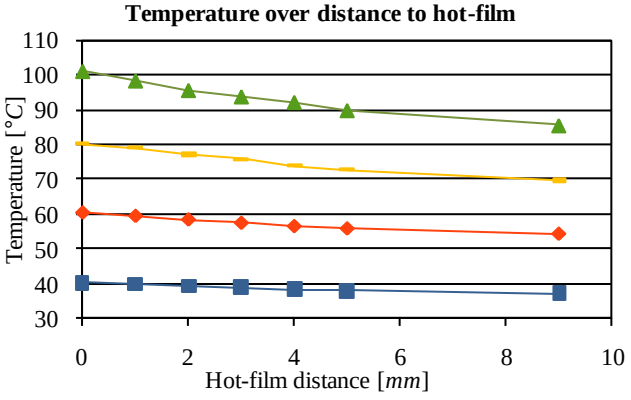

Fig. 10: Silicon substrate temperature T depending on the distance to a hot-film

Because the hot-film is the only module in a multipart sensor which generates heat in the substrate, it is important to know the heat allocation in order to optimize the placement of the other modules and to avoid possible heat disturbances.

Infrared pictures of gold hot-films on silicon were analyzed with a special experimental setup, which included structures for length measurement. All pictures were taken at ambient temperature. The layout is shown in the IR image given in Fig. 9. The gold structures seem to have a lower temperature than the silicon surrounding them. The cause for this effect is the varying emission coefficients of silicon and gold. Hence, the measured temperatures in silicon areas have comparable values.

Because of the high thermal conductivity of silicon ($\lambda_{Si} = 156\ W/(mK)$, [HUL99]) the entire area around the hot-film is heated to temperatures near that of the hot-film.

As shown in Fig. 10 the bulk temperature remains close to the hot-film's temperature, although the distances are relatively high. One can see that the major temperature decrease takes place over the first 4 *mm*. On glass specimens the same effect can be obtained, but in a reduced dimensions, due to the low thermal conductivity of Pyrex glass 7740 ($\lambda_{7740} = 1{,}318\ W/(mK)$, [ASS08]) compared to silicon.

This information leads to the fact that the surrounding modules should be placed at least 4 *mm* from the hot-film. They must also be able to withstand large changes in temperature, if the hot-film is not driven in CTA mode or if it is driven in a pulsed mode. Another (additional) solution could be to insulate the hot-film from the substrate in order to reduce the substrate heat transfer and the influence on other sensor modules. A disadvantage of insulation would be the extended surface warping, which leads to a disturbed flow and consequently to a loss of detection accuracy.

4. Results

The following results were obtained from preliminary tests on the manufactured hot-films. The results of CTA and CCA modes have been compared (Fig. 13).

During the first version of the tests, the output current of the CTA method for different airspeeds has been measured. The diagram below shows the results of these tests, where ΔI refers to is the following equation:

$\Delta I = I(v) - I(v = 0)$. Therefore the offset is zero.

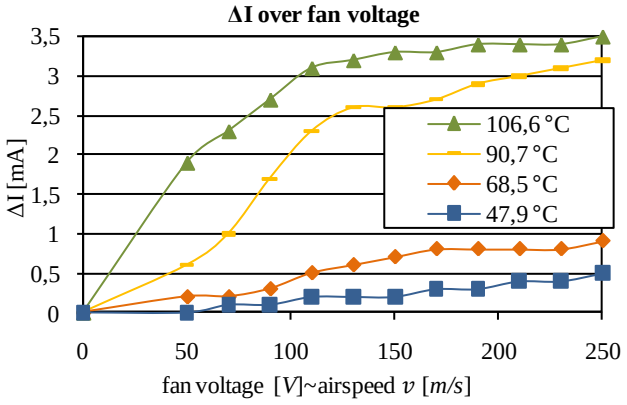

Fig. 11: ΔI over airspeed v indicated by supply voltage of the fan measured by CTA method

Fig. 12 shows the results obtained from the CCA method. The offset at maximum fan voltage is proportional to the air speed which can be determined from the following equation:

$$\Delta U = U(v) - U(v = max).$$

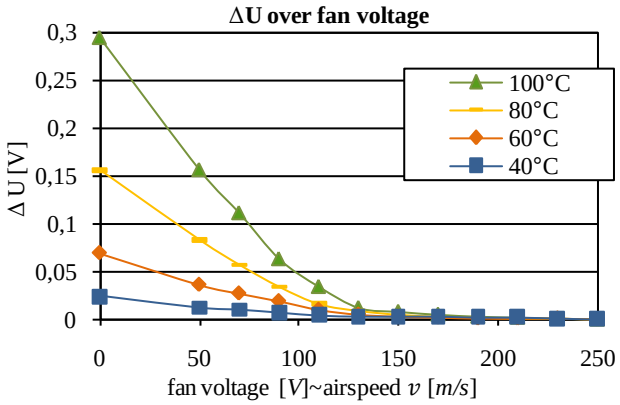

Fig. 12: ΔU over airspeed v indicated by supply voltage of the fan measured by CCA method

A further test was conducted in order to measure the time constant of the film heating. We can see that the time constant increases with an increase in hot-film length. Also the substrate plays an important role. The measurements still have to be refined.

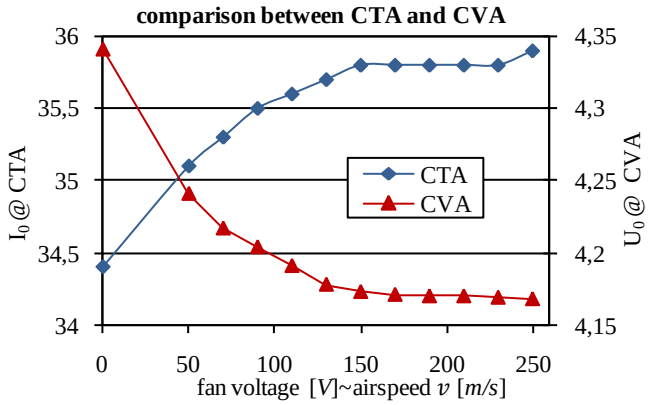

Fig. 13: Comparison of the results from CTA and CCA

5. Conclusions & Outlook

After the completed development of various hot-film geometries, different layouts have been produced in the institute's clean room. A set of hot-films with a wide range of geometries and materials have been created on two different substrates. These layouts have eight different lengths each having four different widths. These films have been manufactured using four different metals which have different electrical behaviors. Additionally, very robust circuits had to be developed in order to operate the hot-films, due to the large range of R_H pertaining to the facts mentioned above.

A basis for an improved layout for the next generation of hot-films has been created. In future work new mask layouts may be easily produced, where the R_0 values may be held constant for various materials. This will enable more precise circuits for improved measurements.

Until now, only one material has been used for the conducting wires and the hot-films. In the future a mix of materials will be used. A simultaneous reduction in the zero sequence resistance and an increase in hot-film resistance must be realized. Conducting wires made of gold, which lead to thin hot-films made of nickel are conceivable.

The variation of material thickness has, until this point not been investigated. In the future the thickness of each layer may be individually set in order to obtain well proportioned sensors.

The determination of the heat allocation near the hot-film leads to new issues in the design process of our multi module sensor. Specifically, the offset of the various modules and there compatibility with changing ambient temperatures must be taken into account. Additionally, dynamic tests with changing or pulsing hot-film temperatures have to be conducted in order to obtain more accurate signals and to allow a further insight into our first hot-film sensors.

The IR camera temperature measurements must be optimized in the future in order to reduce the influence of the different emission and transmission coefficients for IR radiation of the hot-film and substrate materials. For realistic dynamic calibration in fluids, a measurement campaign in a calibrated water tunnel is planned. In the far future the sensor will be integrated on various sensing modules.

ACKNOWLEDGEMENT

This work was funded by the German Research Foundation in the framework of the collaborative research center 880 "Fundamentals of High Lift for Future Civil Aircraft".

REFERENCES

ASM90 ASM; "ASM Handbook: Properties and Selection: Nonferrous Alloys and Special-Purpose Materials" Vol. 2, ASM International, ISBN-10: 0871703785, 1990.

ASS08 Assael, M., Antoniadis, K. and Wu, J.; "New Measurements of the Thermal Conductivity of PMMA, BK7, and Pyrex 7740 up to 450K", Int. Journal of Thermophysics, Vol. 29, Num. 4, pp. 1257-1266, Springer Netherlands, DOI: 10.1007/s10765-008-0504-z, 2008.

BEU10 Beutel, T., Leester-Schädel, M., Wierach, P., Sinapius, M. and Büttgenbach, S.; "Novel Pressure Sensor for Aerospace Purposes" IFSA, Sensors & Transducers Journal Vol. 115, Issue 4, pp.11-19, ISSN 1726-5479, 2010.

ECK97 Eckelmann, H.; "Einführung in die Strömungsmeßtechnik", 1. Auflage, Teubner Verlag, ISBN-10: 3519023792, 1997.

FAR68 Farrel, T, and Greig, D.; „The electrical resistivity of nickel and its alloys" Journal of Physics C: Solid State Physics 1; pp. 1359-1369, DOI: 10.1088/0022-3719/1/5/326, 1968.

HER09 Hering, E., Martin, R., Stohrer, M.; "Physik für Ingenieure", 10. Auflage, Springer Verlag Berlin, ISBN-10: 3540718559, 2008.

HUL99 Hull, R.; "Properties of crystalline silicon", INSPEC London; EMIS datareviews series, No. 20, pp. 165-167, ISBN-10: 0852969333, 1999.

NIT06 Nitsche, W.; „Strömungsmesstechnik", 2. Auflage, Springer Verlag Berlin, ISBN-10: 3540209905, 2006.

KIN14 King, L.V.; "On the convection of heat from small cylinders in a stream of fluid - Determination of convection constants of small platinum wires with application to hot wire anemometry", Philosophical Transactions of the Royal Society, London, Ser. A, Vol. 214, pp. 373-432, 1914.

TRO07 Tropea, C., Yarin, A., Foss, J.; "Handbook of Experimental Fluid Mechanics", 1. Auflage, Springer Verlag Berlin, ISBN-10: 3540251413, 2007.